

## COMPARATIVE INVESTIGATION OF RESONANCE CHARACTERISTICS AND ELECTRICAL SIZE OF THE DOUBLE-SIDED SRR, BC-SRR AND CONVENTIONAL SRR TYPE METAMATERIALS FOR VARYING SUBSTRATE PARAMETERS

E. Ekmekci <sup>†</sup> and G. Turhan-Sayan

Electrical and Electronics Engineering Department  
Middle East Technical University  
Ankara, Turkey

**Abstract**—This paper introduces a planar  $\mu$ -negative (MNG) metamaterial structure, called double-sided split ring resonator (DSRR), which combines the features of a conventional SRR and a broadside-coupled SRR (BC-SRR) to obtain much better miniaturization at microwave frequencies for a given physical cell size. In this study, electromagnetic transmission characteristics of DSRR, BC-SRR and conventional SRR are investigated in a comparative manner for varying values of substrate parameters which are thickness, the real part of relative permittivity and dielectric loss tangent. Simulation results have shown that magnetic resonance patterns of all these three structures are affected in a similar way from variations in permittivity and in loss tangent. However, changes in substrate thickness affect their resonance characteristics quite differently: In response to decreasing substrate thickness, resonance frequency of the SRR increases slowly while the bandwidth and the depth of its resonance curve do not change much. For the DSRR and BC-SRR structures, on the other hand, resonance frequency, half power bandwidth and the depth of resonance curve strongly decrease with decreasing substrate thickness. Among these three structures, all having the same unit cell dimensions, the newly suggested DSRR is found to reach the lowest resonance frequency, hence the smallest electrical size, which is a highly desired property not only for more effective medium approximation but also for miniaturization in RF design. The BC-SRR, on the other hand, provides the largest

---

Corresponding author: E. Ekmekci (eekmekci@metu.edu.tr).

<sup>†</sup> Also with Electronics and Communication Engineering Department, Suleyman Demirel University, Isparta, Turkey.

resonance bandwidth which is almost three times of the resonance bandwidth of the SRR. The bandwidth of the DSRR approaches to that of the BC-SRR as the planar separation between its inner and outer rings increases.

## 1. INTRODUCTION

As suggested by Veselago in late 60's, left-handed metamaterials are artificial materials designed to have simultaneously negative values of permeability and permittivity over a finite frequency band [1]. Such an artificial medium can be realized by using periodical arrays of SRRs and thin-wires together where the SRR array is used to obtain negative values of effective permeability while the thin-wire array serves to produce negative values of effective permittivity as shown by the studies of Pendry et al. [2, 3] and Smith et al. [4]. Although the conventional SRR is not the only magnetic resonator suggested in literature with  $\mu$ -negative property, it has been the most widely studied metamaterial structure so far. Effects of fundamental SRR parameters (metal width, split width, separation between the rings, etc.) on the resonance frequency of the structure were studied by Weiland et al. [5], Aydin et al. [6] and Wu et al. [18] for example. Possibility of tuning the resonance frequency of SRRs by changing the permeability and permittivity of the surrounding medium was discussed in [5] in 2001. Recently, effects of substrate thickness and substrate permittivity for tuning the SRR's resonance frequency were studied in detail by Sheng et al. [7]. While the behavior of complex metamaterial structures can be investigated accurately by using sophisticated full-wave electromagnetic analysis methods, the use of proper equivalent circuit models for such structures would certainly simplify the analysis and design task. In 2004 and 2005, Baena et al. proposed and verified an equivalent circuit model for the SRR unit cell neglecting the effects of small slit capacitances and dielectric losses [8, 14]. Also in 2005, Yao et al. characterized two dimensional isotropic metamaterials fabricated from cross split-ring resonators and studied their constitutive relation tensors [19]. In 2006, Chen et al. proposed an equivalent circuit model for the unit cell of a three-dimensional array of ring type magnetic resonators including the coupling effects between individual columns of rings in the model [9]. Effects of dielectric losses as well as conductor losses were represented in the equivalent circuit models suggested recently by Bilotti et al. for the structures of multiple SRRs with single and double slits and for spiral resonators [10]. Besides, Cui et al. proposed a symmetrical circuit

model describing all kinds of circuit metamaterials [20].

In 2002, Marqués et al. studied the electromagnetic polarizabilities of the conventional SRR to reveal its bianisotropic nature and they also proposed a modified SRR structure to avoid bianisotropy [11]. The modified SRR was composed of two identical metallic rings printed and aligned on opposite faces of a dielectric substrate where their slit locations were 180 degrees apart. Later in 2003, Marqués et al. revisited the analysis of the conventional SRR and the modified SRR, which were called edge-coupled SRR (EC-SRR) and broadside-coupled SRR (BC-SRR), respectively in [12]. In that paper, variation of the resonance frequency with metal strip width and with overall cell-size was analyzed for both structures. Also, for several different values of substrate permittivity, dependence of the resonance frequency of the EC-SRR on ring separation was investigated as well as the dependence of resonance frequency of the BC-SRR on the substrate thickness. Based on the detailed analyses conducted in [12], it was concluded that the BC-SRR had the advantage of having a much smaller electrical size as compared to the conventional SRR [11].

Magnetic resonator topologies other than the conventional SRR and BC-SRR have also been suggested in literature. Conventional spiral resonator (SR) topology, in particular, was shown to provide a much smaller electrical size in various studies [8, 10, 17] as compared to the conventional SRR topology. Double sided or broadside coupled SR topologies have been also suggested recently in [21, 22] and [25]. In 2007, Aznar et al. studied metamaterial transmission lines based on broadside coupled spiral resonators. They showed that the electrical size of metamaterial resonator structures could be reduced by combining spiral topologies with broadside coupling [21]. Based on this idea, they proposed some novel broad-side coupled spiral resonator (BC- SR) structures by using two metal layers connected by conducting vias, in 2008 [22]. It is also discussed in [22] that the resonance frequency (and hence the electrical size of the resonating particle) can be considerably reduced for smaller substrate thicknesses in either spiral resonators or in coupled two-resonator topologies as a result of increased broadside coupling. The smallest electrical size reported in [22] belongs to a broadside coupled SR topology with a small substrate thickness, which is about ten percent of the electrical size of a conventional SRR. Also, in 2008, Ekmekci et al. demonstrated the usefulness of the double-sided spiral resonator (DSR) and the novel double-sided U-spiral resonator (DUSR) topologies with broadside coupling for miniaturization especially for larger number of turns [25]. These topologies do not have any conductive connection between the metallic inclusions printed on opposing faces of the substrate. For

a turn number of six, the electrical size of the DSR was about ten percent of the electrical size of the conventional SRR. This ratio was even smaller, nine percent, for the DUSR. Even smaller electrical sizes are anticipated with the DSR and DUSR topologies for the number of turns larger than six. However, it should be mentioned that reduction rate in resonance frequency is known to slow down and finally becomes almost zero as the turn number keeps increasing as reported by Bilotti et al. for conventional (single-sided) spiral resonators in [17].

In this work, we describe a novel-negative magnetic resonator by combining the EC-SRR (i.e., conventional SRR) and the BC-SRR particles to form the double-sided SRR (DSRR) structure. For this resonator topology, the preliminary research results (regarding the variation of resonance frequency with the thickness and permittivity of substrate) were presented recently in a conference paper by Ekmekci et al. [15]. In the present paper, we propose a novel  $\mu$ -negative magnetic resonator by combining the EC-SRR (i.e., conventional SRR) and the BC-SRR particles to form the double-sided SRR (DSRR) structure. Using full-wave electromagnetic analysis, transmission characteristics of the DSRR, BC-SRR and SRR are investigated in a comparative manner to figure out the advantages of this newly suggested magnetic resonator, the DSRR, over the already existing alternatives. For each structure, the resonance parameters, i.e., the resonance frequency ( $f_0$ ), half power bandwidth (*HPBW*) and the depth of resonance curve ( $T_{\min}$ ), are extracted from the spectra of the scattering parameter  $S_{21}$  for varying values of substrate parameters which are the substrate thickness ( $d$ ), real part of relative permittivity ( $\epsilon_r$ ) and dielectric loss tangent ( $\tan\delta_c$ ). Numerical simulations are conducted using the Ansoft's HFSS software which makes use of the finite elements method. It will be demonstrated that among these three structures, all with the same unit cell dimensions, the newly suggested DSRR is found to reach the lowest resonance frequency, hence the smallest electrical size. Obviously, reducing the electrical size in metamaterial design is a very important goal as it leads to a more effective medium approximation and a higher degree of device miniaturization in microwave applications. Another important concern in magnetic resonator design is the resonance bandwidth. It will be shown that the BC-SRR provides the largest resonance bandwidth which is almost three times of the resonance bandwidth of the SRR. The bandwidth of the DSRR, on the other hand, approaches to that of the BC-SRR as the planar separation between its inner and outer rings increases.

The particular aim of this paper is to investigate the resonance properties of the DSRR topology and compare them with those of

the closely related SRR and the BC-SRR topologies to show that using broadside coupling (provided by the BC-SRR) together with edge coupling (provided by the conventional SRR) gives us a higher degree of freedom to control the resonance parameters (such as the resonance frequency and bandwidth) by changing the substrate parameters. Resonance parameters of the other magnetic resonator structures such as the conventional (i.e., single sided) or double sided spiral, U-spiral and Multiple SRR topologies will be investigated in detail in a comparative manner in a future publication which is under preparation.

## 2. DESCRIPTION OF THE RESONATOR TOPOLOGIES, STRUCTURAL PARAMETERS AND THE SIMULATION SETUP

### 2.1. Description of the Geometry, Structural Parameters and the Simulation Setup

The unit cell geometries used for the SRR, BC-SRR and DSRR structures are described in Figures 1(a), 1(b) and 1(c), respectively, where the overall cell sizes as well as the split ring dimensions are kept the same for all three structures for fair comparison of the simulation results. The unit cells shown in Figure 1 have the common geometrical parameters of  $L = 5$  mm (side length of the square shaped substrate surface),  $l = 4$  mm and  $h = 3$  mm (side lengths of the rectangular shaped outer ring),  $g = 0.5$  mm (gap distance or slit length) and  $w = 0.3$  mm (width of the metal ring). The rings of the resonators are made of copper lines with the metal thickness of 0.03 mm and conductivity of  $5.8 \times 10^7$  S/m. The parameter  $s$  refers to the planar

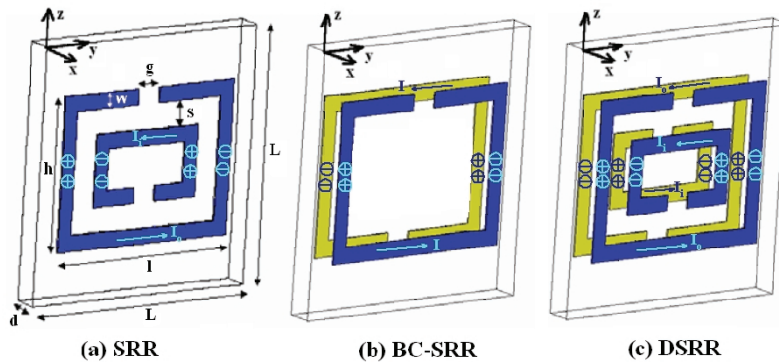


**Figure 1.** Unit cell geometries for the SRR, BC-SRR, and DSRR type metamaterials.

separation distance between the inner and outer rings of the SRR and DSRR structures in Figures 1(a) and 1(c), respectively. Two different values of this parameter,  $s = 0.2$  and  $s = 0.5$  mm, are used in simulations to show the advantage of using the DSRR structure rather than using the SRR or BC-SRR to obtain smaller resonance frequencies or wider bandwidths. As seen in Figure 1(b), the BC-SRR structure consists of two rings, which are the same as the outer ring of the conventional SRR, aligned over the opposite faces of the substrate in an inverted position. The parameter  $s$  is not applicable to the BC-SRR as it has no inner ring. The DSRR unit cell shown in Figure 1(c), on the other hand, consists of two identical SRR patterns aligned over the opposite faces of the substrate in an inverted fashion. It will be assumed in the simulations that all three structures are designed using the same lossy dielectric substrate. The relative permeability of the substrate  $\mu_r$  is taken to be unity. The other substrate parameters, i.e., thickness ( $d$ ), real part of relative permittivity ( $\epsilon_r$ ), and loss tangent ( $\tan \delta_c$ ) will be treated as variables in the simulations.

In Figure 1, we also indicate the directions of induced ring currents and the polarities of associated charge distributions due to an externally applied time varying magnetic field whose direction is perpendicular to the planes of metallic inclusions. For the SRR structure, there is a non-zero electric polarization (along  $-y$  direction) due to the applied magnetic field as implied by the polarities of induced charge distributions in Figure 1(a). However, net electric polarization is produced due to applied external magnetic field in the BC-SRR and DSRR topologies. Therefore, the SRR topology has bianisotropy [11] but the BC-SRR and DSRR topologies are non-bianisotropic.

Resonance characteristics of the SRR, BC-SRR and DSRR unit cells can be investigated using their transmission spectra. A typical transmission versus frequency curve is shown in Figure 2 where the definitions of resonance parameters  $f_0$ ,  $HPBW$  and  $T_{\min}$  are indicated. The complex scattering parameter  $S_{21}$  for a given unit cell must be computed to obtain its transmission spectrum. The reflection spectra, i.e., the complex scattering parameter  $S_{11}$  is also needed if the effective medium parameters  $\epsilon_{eff}$  and  $\mu_{eff}$  are to be extracted [13]. In this work, the complex scattering parameters are computed using the Ansoft's HFSS software which is based on the finite elements method.

The simulation setup used for HFSS computations is described in Figure 3 where the unit cell is surrounded by air medium and the  $z$ -polarized incident electromagnetic plane wave propagates along the  $y$  direction. Hence, the direction of the magnetic field vector is along the  $x$  axis that is perpendicular to the resonator

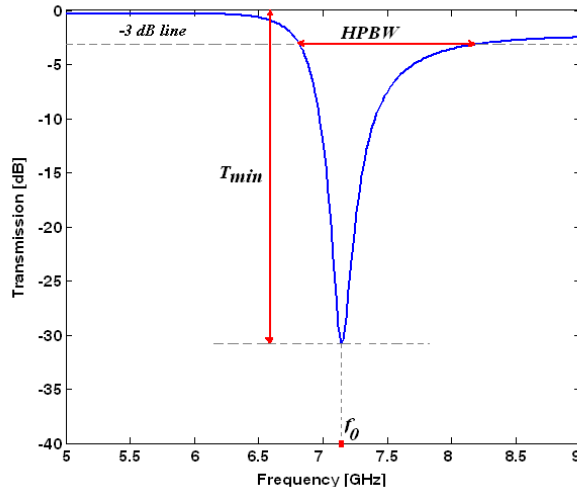


**Figure 2.** Resonance parameters (i.e.,  $f_0$ ,  $HPBW$ , and  $T_{min}$ ) defined on the transmission versus frequency curve.

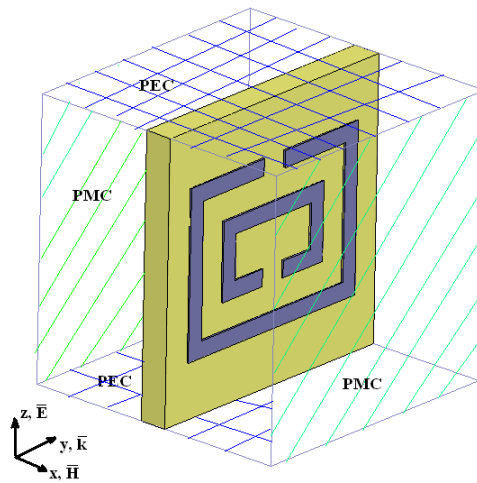


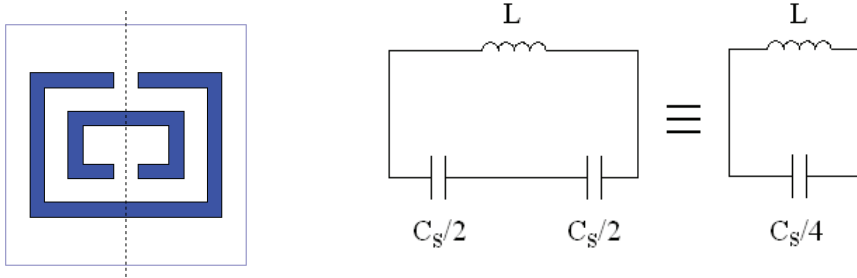
**Figure 3.** Setup for HFSS simulations.

plane. Perfect electric conductor (PEC) boundary conditions are applied along the boundaries perpendicular to the  $z$  axis and perfect magnetic conductor (PMC) boundary conditions are applied along the boundaries perpendicular to the  $x$  axis. The remaining two boundaries are assigned to be the input-output wave ports. HFSS simulations are performed with 0.02 GHz incremental steps. Using a single unit cell

together with the boundary conditions stated above, one can model an infinite periodic array of structures as discussed in [5, 23].

## 2.2. Equivalent Circuit Models

Earlier studies on the conventional SRR have shown that this structure behaves as an LC resonator with the resonance frequency  $\omega_0 = 2\pi f_0 = 1/\sqrt{LC}$ . Methods for the calculation of the equivalent inductance  $L$  and the equivalent capacitance  $C$  of the SRR structure in the presence of a dielectric substrate were suggested in [12]. Theory established in this work was further elaborated by Baena et al. in [8, 14] to show that the total distributed capacitance  $C$  between the inner and the outer rings of the SRR can be calculated from the series connection of two equal valued capacitances ( $C_s/2$ ) associated with each symmetrical halves of the structure. The symmetry line of the SRR passes through the gap locations of the inner and outer rings as shown in Figure 4(a). Therefore, the simplest equivalent circuit model (neglecting losses) for the SRR unit cell looks like the one given in Figure 4(b) where  $C = C_s/4$ . Calculation of the parameters  $L$  and  $C_s$  in the presence of a dielectric substrate is also discussed in [10] by Bilotti et al. in addition to references [8, 12].



(a) SRR geometry with symmetry line      (b) Equivalent circuit model

**Figure 4.** The conventional SRR topology with its symmetry line and its equivalent circuit model.

In the present paper, we propose a very simple equivalent circuit model for the newly suggested DSRR unit cell to explain the basic relations between the substrate parameters (substrate thickness and substrate relative permittivity) and the resonance frequency  $f_0$  as shown in Figure 5. In this model, we neglect the conductor and dielectric losses and the inductive coupling effects between the neighboring DSRR cells. These issues will be the subjects of a future work.

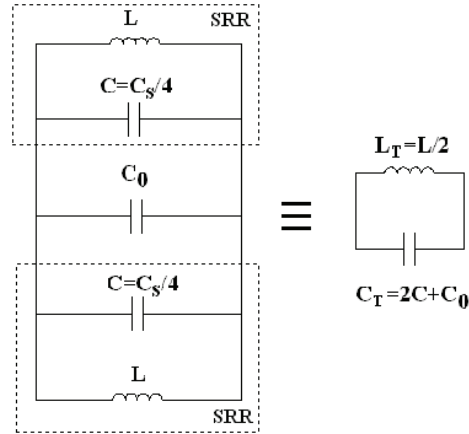


**Figure 5.** A simple equivalent circuit model for the DSRR unit cell.

The equivalent circuit model for the DSRR is composed of the parallel connection of two identical SRR equivalent circuits and a capacitor with capacitance value  $C_0$ . This capacitor represents the cross coupling effect due to the conducting strips printed on opposite faces of the substrate. The value of  $C_0$  can be computed by using the approximate formula given in equation (1)

$$C_0 = \frac{\varepsilon_0 \varepsilon_r A}{8d} \tag{1}$$

where  $\varepsilon_r$  and  $d$  are the real part of relative permittivity and the thickness of the substrate, respectively, and  $A$  is the total conducting strip area on one face of the substrate including both the inner and the outer rings. This expression is basically the approximate form of the parallel-plate capacitance formula used in [9] to compute the broadside capacitance except an empirically determined factor (1/8). Then, due to the parallel connections, the total capacitance  $C_T$  and the total inductance  $L_T$  of the DSRRs equivalent circuit model become

$$C_T = 2C + C_0 \tag{2}$$

and

$$L_T = L/2 \tag{3}$$

Therefore, the resonance frequency of the DSRR cell can be computed

from

$$f_0 = \frac{1}{2\pi\sqrt{L_T C_T}} \quad (4)$$

Although the equivalent circuit model introduced above is suggested for the DSRR cell, it is also useful to model the BC-SRR cell provided that the absence of the inner conducting ring is accounted for in the computation of the  $L$  and  $C$  terms. In the absence of the inner ring, the capacitance  $C$  must be composed of the gap capacitance  $C_g$  which is negligibly small as compared to the capacitance between the inner and outer rings of the SRR unit cell. It is also negligible in comparison to  $C_0$  which is the dominating capacitance term unless the substrate thickness becomes too large. Also, value of the  $C_0$  is expected to be smaller in the BC-SRR model due to a smaller metal strip area  $A$ .

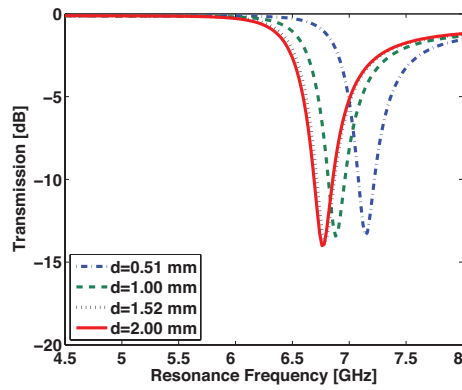
The equivalent circuit model suggested for the DSRR will be verified in Section 5 after obtaining the results of the relevant HFSS simulations for various substrate parameters in Section 3.

### 3. SIMULATION OF THE RESONANCE BEHAVIOR FOR THE SRR, BC-SRR AND DSRR CELLS

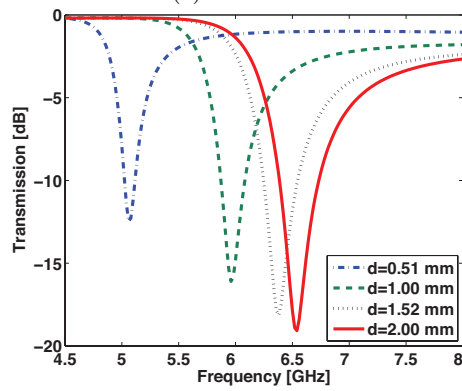
Earlier studies on the comparison of conventional SRR and BC-SRR structures [11, 12] inspired us to suggest the DSRR type magnetic resonator topology [15] which has the additional flexibility to achieve better miniaturization provided by its double-sided structure (like the BC-SRR) with the presence of inner rings (like the conventional SRR). Detailed comparison of the DSRR, BC-SRR and conventional SRR will be presented in this section regarding the effects of substrate parameters on the resonance characteristics of these closely related metamaterial structures.

#### 3.1. Effects of the Substrate Thickness ( $d$ ) on Resonance Parameters

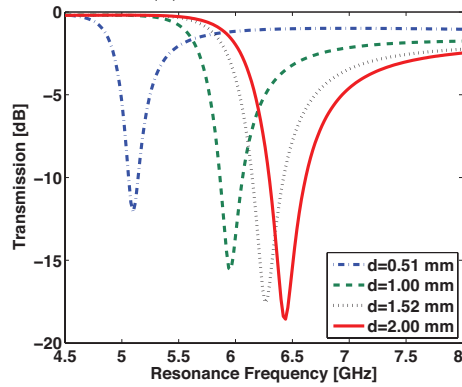
Transmission spectra of the SRR, BC-SRR and DSRR unit cells are numerically computed by the HFSS software, using the structural parameter values stated in Section 2.1 with  $s = 0.5$  mm, for different values of the substrate thickness  $d = 0.51, 1.00, 1.52, 2.00$  mm. In the meantime, the other substrate parameters are kept constant at values  $\epsilon_r = 4.4$  and  $\tan \delta_c = 0.020$ . These simulations are also repeated for the SRR and DSRR structures with  $s = 0.2$  mm. The resulting parametric curves of transmission versus frequency are plotted in Figures 6(a), 6(b) and 6(c) for the SRR, BC-SRR and DSRR cells, respectively. The



(a) SRR case



(b) BC-SRR case



(c) DSRR case

**Figure 6.** Transmission spectra of the SRR, BC-SRR and DSRR unit cells for different substrate thicknesses using  $L = 5$  mm,  $l = 4$  mm,  $h = 3$  mm,  $g = 0.5$  mm,  $w = 0.3$  mm,  $s = 0.5$  mm,  $\epsilon_r = 4.4$  and  $\tan \delta_c = 0.020$ .

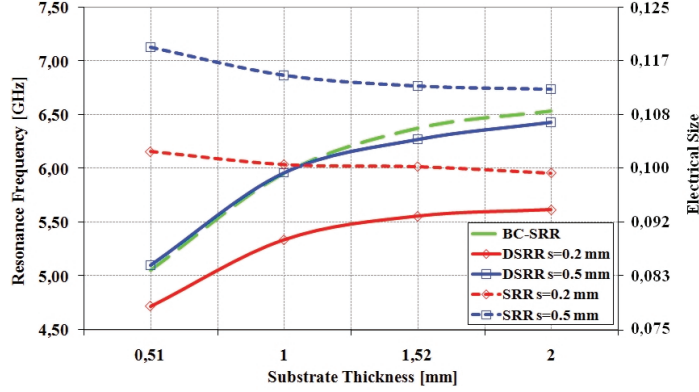


**Figure 7.** Variation of the resonance frequency ( $f_0$ ) and electrical size ( $u$ ) with substrate thickness ( $d$ ) for the SRR, BC-SRR and DSRR unit cells using  $L = 5$  mm,  $l = 4$  mm,  $h = 3$  mm,  $g = 0.5$  mm,  $w = 0.3$  mm,  $\epsilon_r = 4.4$  and  $\tan \delta_c = 0.020$ .

resonance frequency ( $f_0$ ), half-power resonance bandwidth ( $HPBW$ ) and transmission minimum ( $T_{\min}$ ) values are extracted from each of the transmission curves presented in Figure 6. Then, these values are sorted and plotted in Figures 7, 8 and 9 as  $f_0$  versus  $d$ ,  $HPBW$  versus  $d$  and  $T_{\min}$  versus  $d$  curves, respectively. Based on the simulation results presented in Figures 6 through 9, we make the following observations:

### 3.1.1. Variation of the Resonance Frequency ( $f_0$ ) with $d$ :

- As the substrate thickness  $d$  increases from 0.51 to 2 mm, the resonance frequency  $f_0$  of the SRR unit cell decreases slowly from 7.13 GHz to 6.74 GHz for  $s = 0.5$  mm as seen in Figure 4(a) and Figure 5. This behavior of  $f_0$  is expected as the capacitance term  $C_s$  in the SRR model (see Figure 4(b)) increases as  $d$  gets larger [10].
- On the other hand, the  $f_0$  versus  $d$  curves of BC-SRR and DSRR unit cells display a totally different behavior; they both strongly increase with increasing substrate thickness as seen in Figures 6(b), 6(c) and Figure 7. As  $d$  increases from 0.51 to 2 mm,  $f_0$  of the BC-SRR cell increases from 5.06 to 6.54 GHz almost exponentially. For  $s = 0.5$  mm case, the  $f_0$  versus  $d$  curve of the DSRR is very similar to that of the BC-SRR as shown in Figure 7. This behavior can be explained as follows: Comparing the equivalent circuit models in Figure 4(b) and Figure 5, we can see that increasing  $d$  only affects  $C$  in the SRR model; however

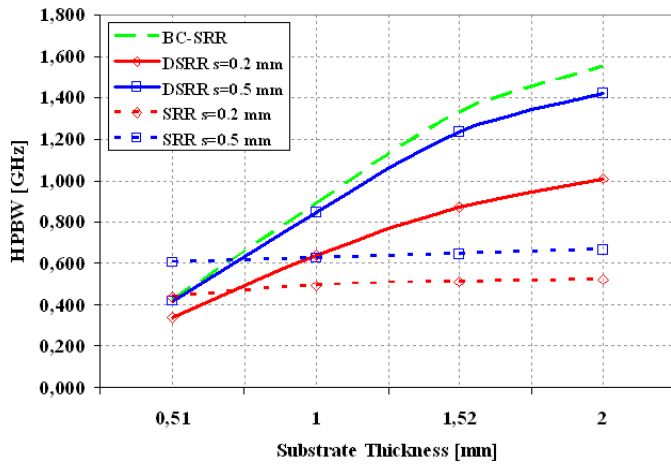


**Figure 8.** Variation of the resonance bandwidth ( $HPBW$ ) with substrate thickness ( $d$ ) for the SRR, BC-SRR and DSRR unit cells using  $L = 5$  mm,  $l = 4$  mm,  $h = 3$  mm,  $g = 0.5$  mm,  $w = 0.3$  mm,  $\epsilon_r = 4.4$  and  $\tan \delta_c = 0.020$ .

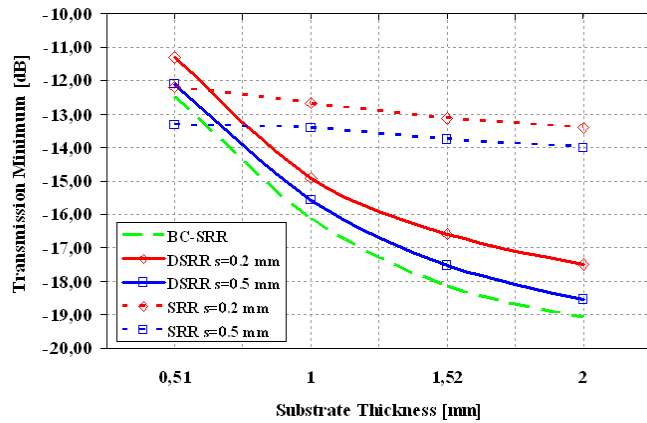


**Figure 9.** Variation of the transmission minimum ( $T_{min}$ ) with substrate thickness ( $d$ ) for the SRR, BC-SRR and DSRR unit cells using  $L = 5$  mm,  $l = 4$  mm,  $h = 3$  mm,  $g = 0.5$  mm,  $w = 0.3$  mm,  $\epsilon_r = 4.4$  and  $\tan \delta_c = 0.020$ .

it affects both  $C$  and  $C_0$  in BC-SRR and DSRR models. For an increase in  $d$ , the value of  $C$  increases but  $C_0$  decreases (see equation (1)). However, the capacitance  $C_0$  is more dominant than  $C$ . Therefore, the total capacitance  $C_T$  in equation (2) decreases and hence  $f_0$  of the BC-SRR and DSRR cells increases.

- The  $f_0$  versus  $d$  curves of the SRR and DSRR unit cells can be shifted to lower frequency levels by reducing the planar separation distance,  $s$ , between the rings. As seen in Figure 7, for  $s = 0.2$  mm case,  $f_0$  of the SRR unit cell decreases from 6.16 to 5.96 GHz and  $f_0$  of the DSRR unit cell increases from 4.72 to 5.62 GHz as  $d$  increases from 0.51 to 2 mm. In fact, reducing  $s$  while keeping all the other parameters (including  $d$ ) fixed leads to higher  $C_s$  values [10]. Therefore, the total capacitance  $C = C_s/4$  in the SRR model and the total capacitance  $C_0 + (C_s/2)$  in the DSRR model both increase leading to smaller  $f_0$  values. It is important to note that the BC-SRR is much better than the SRR cell in terms of miniaturization but it cannot use the tuning advantage of the parameter  $s$ . The DSRR structure, however, can have much smaller values of resonance frequency than those of the BC-SRR just by reducing the  $s$  parameter.

*Conclusion 1:* The novel DSRR cell is superior to the SRR and BC-SRR cells in terms of miniaturization as it can provide much smaller resonance frequency values. The degree of miniaturization can be adjusted by tuning the substrate thickness and the planar separation between the rings when all the other parameters are fixed. For example, a reduction of 28.5% is obtained in  $f_0$  (reduction from 7.13 GHz to 5.10 GHz) for  $d = 0.51$  mm and  $s = 0.5$  mm by using DSRR instead of SRR. Reduction in resonance frequency becomes 23.4% (from 6.16 GHz to 4.72 GHz) if  $s = 0.2$  mm is used instead. Also, reduction in  $f_0$  is more pronounced for smaller  $s$  values and thicker substrates when the DSRR and BC-SRR structures are compared. For instance, the reduction in  $f_0$  is almost zero when  $s = 0.5$ , but it is 14% for  $s = 0.2$  at  $d = 2$  mm and only 6.7% for  $s = 0.2$  and  $d = 0.51$  mm.

### 3.1.2. Variation of the Half-power Bandwidth (HPBW) with $d$ :

- As the substrate thickness  $d$  increases from 0.51 to 2 mm, the *HPBW* of the SRR increases very slightly. Practically, we can assume that the *HPBW* versus  $d$  curve of the SRR remains almost constant about 0.6 GHz for  $s = 0.5$  mm and about 0.45 GHz for  $s = 0.2$  mm (see Figure 8).
- The *HPBW* versus  $d$  curve of the BC-SRR shows the largest increase from 0.43 to 1.55 GHz as shown in Figure 8.

- The *HPBW* versus  $d$  curve of the DSRR displays a similar behavior as that of the BC-SRR. For small  $s$  values, the *HPBW* of the DSRR becomes smaller than that of the BC-SRR. For  $s = 0.2$  mm, for instance, the *HPBW* of the DSRR increases from 0.34 to 1.01 GHz. As the planar separation distance between the rings increases, however, the *HPBW* versus  $d$  curve of the DSRR converges to that of the BC-SRR as shown in Figure 8.

*Conclusion 2:* The BC-SRR cell is superior to the SRR and DSRR cells in terms of having a larger resonance bandwidth. However, the bandwidth performance of the novel DSRR cell gets very close to that of the BC-SRR. In fact *HPBW* is one of the most important parameters in metamaterial structures, because an increase in *HPBW* increases the frequency band with negative permeability, hence increases the left-handed region.

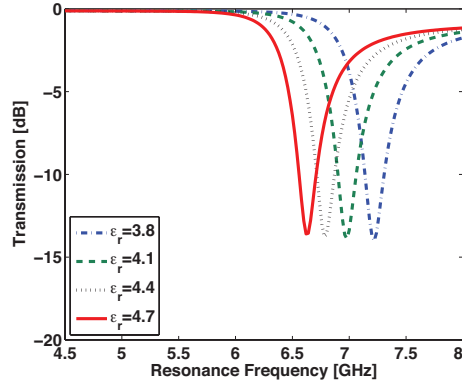
### 3.1.3. Variation of the Transmission Minimum ( $T_{\min}$ ) with $d$ :

As the substrate thickness  $d$  increases from 0.51 to 2 mm,  $T_{\min}$  of the SRR decreases very slightly from  $-13.33$  to  $-14$  dB for  $s = 0.5$  mm, and from  $-12.18$  to  $-13.41$  dB for  $s = 0.2$  mm (see Figure 6(a) and Figure 9).

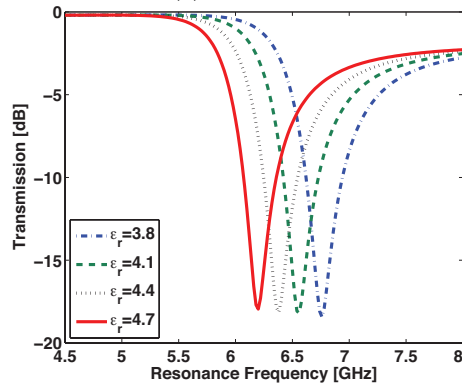
The  $T_{\min}$  versus  $d$  curves of the DSRR and BC-SRR cells, however, decrease sharply by more than 6 dB (roughly from  $-12$  dB to  $-18$  dB) as  $d$  increases from 0.51 to 2 mm as shown in Figures 6(b), 6(c) and Figure 9.

## 3.2. Effects of the Relative Permittivity ( $\epsilon_r$ ) of the Substrate on Resonance Parameters

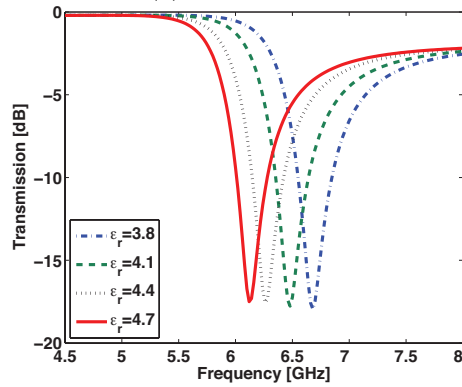
Transmission spectra of the SRR, BC-SRR and DSRR unit cells are numerically computed by the HFSS software, using the structural parameter values stated in Section 2 with  $s = 0.5$  mm, for different values of substrate permittivity. The simulations are conducted for  $\epsilon_r = 3.8, 4.1, 4.4$  and  $4.7$  values while the other substrate parameters are kept constant at  $d = 1.52$  mm and  $\tan \delta_c = 0.020$ . These simulations are also repeated for the SRR and DSRR structures with  $s = 0.2$  mm. The resulting parametric curves of transmission versus frequency are plotted in Figures 10(a), 10(b) and 10(c) for the SRR, BC-SRR and DSRR cells, respectively. The resonance frequency ( $f_0$ ), half-power resonance bandwidth (*HPBW*) and transmission minimum ( $T_{\min}$ ) values are extracted from each of the transmission curves presented in Figure 10. Then, these values are sorted and plotted in Figures 11, 12 and 13 as  $f_0$  versus  $\epsilon_r$ , *HPBW* versus  $\epsilon_r$  and  $T_{\min}$



(a) SRR case



(b) BC-SRR case



(c) DSRR case

**Figure 10.** Transmission spectra of the SRR, BC-SRR and DSRR unit cells for different relative substrate permittivity values of the substrate using  $L = 5$  mm,  $l = 4$  mm,  $h = 3$  mm,  $g = 0.5$  mm,  $w = 0.3$  mm,  $s = 0.5$  mm,  $d = 1.52$  mm and  $\tan \delta_c = 0.020$ .

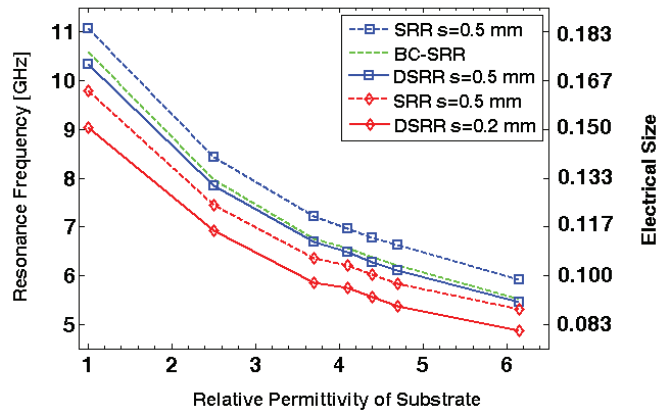


**Figure 11.** Variation of the resonance frequency ( $f_0$ ) and electrical size ( $u$ ) with relative substrate permittivity ( $\epsilon_r$ ) for the SRR, BC-SRR and DSRR unit cells using  $L = 5$  mm,  $l = 4$  mm,  $h = 3$  mm,  $g = 0.5$  mm,  $w = 0.3$  mm,  $d = 1.52$  mm and  $\tan \delta_c = 0.020$ .

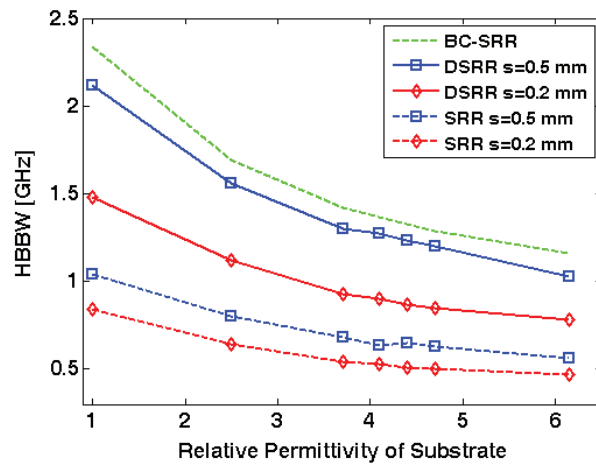


**Figure 12.** Variation of the resonance bandwidth ( $HPBW$ ) with relative substrate permittivity ( $\epsilon_r$ ) for the SRR, BC-SRR and DSRR unit cells using  $L = 5$  mm,  $l = 4$  mm,  $h = 3$  mm,  $g = 0.5$  mm,  $w = 0.3$  mm,  $d = 1.52$  mm and  $\tan \delta_c = 0.020$ .

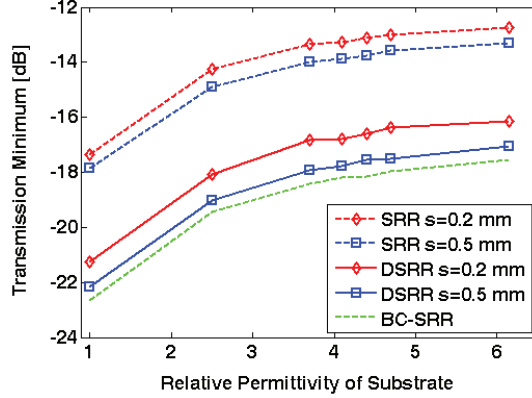


**Figure 13.** Variation of the transmission minimum ( $T_{\min}$ ) with relative substrate permittivity ( $\epsilon_r$ ) for the SRR, BC-SRR and DSRR unit cells using  $L = 5$  mm,  $l = 4$  mm,  $h = 3$  mm,  $g = 0.5$  mm,  $w = 0.3$  mm,  $d = 1.52$  mm and  $\tan \delta_c = 0.020$ .

versus  $\epsilon_r$  curves, respectively. As the range of variation for  $\epsilon_r$  (from 3.8 to 4.7) is quite small, the nonlinear relations between the substrate permittivity and resonance parameters are not revealed in Figure 10. For that reason, additional simulations are run for  $\epsilon_r = 1.0, 2.5$  and  $6.15$ , and the results are presented in Figures 11, 12 and 13 to cover a wider range for  $\epsilon_r$  from 1.0 to 6.15. Based on the simulation results presented in Figures 10 through 13, we make the following observations:

### 3.2.1. Variation of the Resonance Frequency ( $f_0$ ) with $\epsilon_r$

As the relative permittivity  $\epsilon_r$  of substrate increases from 3.8 to 4.7, the resonance frequency  $f_0$  decreases almost linearly and with almost the same slope for all three resonator cells as seen in Figures 10 and 11. When the  $\epsilon_r$  range is extended from 1.0 to 6.15 with additional simulation results, the nonlinearly decreasing behavior in  $f_0$  versus  $\epsilon_r$  curves of SRR, BC-SRR and DSRR structures is observed as expected from the circuit models. In this permittivity range, for the given set of fixed parameter values, the DSRR cell with  $s = 0.2$  mm has the lowest curve of  $f_0$  versus  $\epsilon_r$ . In other words, DSRR provides the smallest electrical size again.

### 3.2.2. Variation of the Resonance Bandwidth (HPBW) with $\epsilon_r$

As seen in Figures 10 and 12, the HPBW versus  $\epsilon_r$  curves of all three resonator cells decrease almost exponentially as  $\epsilon_r$  increases. The BC-

SRR has the largest *HPBW* values in this substrate permittivity range changing from 2.3 to 1.2 GHz. The *HPBW* versus  $\varepsilon_r$  curve of the DSRR with  $s = 0.5$  mm is the second best in providing large *HPBW* values changing from 2.1 to 1.0 GHz. The SRR cell with  $s = 0.2$  mm has the lowest *HPBW* values changing from 0.8 to 0.5 GHz. *HPBW* values of the BC-SRR are almost three times of the *HPBW* values of the SRR under these simulation conditions.

### 3.2.3. Variation of the Transmission Minimum ( $T_{\min}$ ) with $\varepsilon_r$

As shown in Figures 10 and 13, the  $T_{\min}$  versus  $\varepsilon_r$  curves of all three resonators increase almost exponentially as  $\varepsilon_r$  increases from 1.0 to 6.15. Transmission minimum at resonance for the BC-SRR and DSRR cells are smaller by about 4 dB as compared to those of the SRR cell for all  $\varepsilon_r$  values. Smaller  $T_{\min} = |S_{21}|$  at resonance leads to higher unloaded quality factor [22], hence it is the indication of smaller losses.

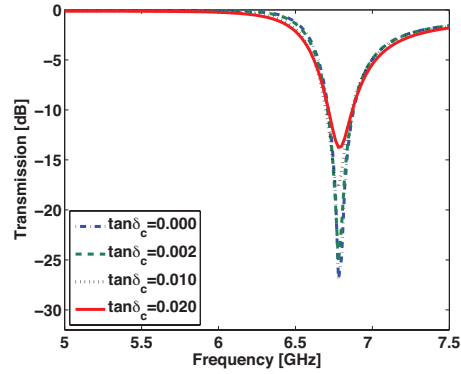
### 3.3. Effects of the Loss Tangent ( $\tan \delta_c$ ) of the Substrate on Resonance Parameters

Transmission spectra of the SRR, BC-SRR and DSRR unit cells are numerically computed by the HFSS software, using the structural parameter values stated in Section 2 with  $s = 0.5$  mm, for different values of substrate loss tangent. The simulations are conducted for  $\tan \delta_c = 0, 0.002, 0.010$  and  $0.020$  while the other substrate parameters are kept constant at  $d = 1.52$  mm and  $\varepsilon_r = 4.4$ . The resulting parametric curves of transmission versus frequency are plotted in Figures 14(a), 14(b) and 14(c) for the SRR, BC-SRR and DSRR cells, respectively. It is seen in Figure 14(a) that the resonance frequency and the bandwidth of SRR do not change noticeably by loss tangent. Only the transmission minimum changes from  $-26.99$  to  $-13.75$  dB as  $\tan \delta_c$  changes from zero to 0.02. In other words, the resonance curve becomes shallower as the losses of the dielectric substrate increases. The similar behavior is observed for BC-SRR and DSRR cells also as seen in Figures 14(b) and 14(c), respectively.

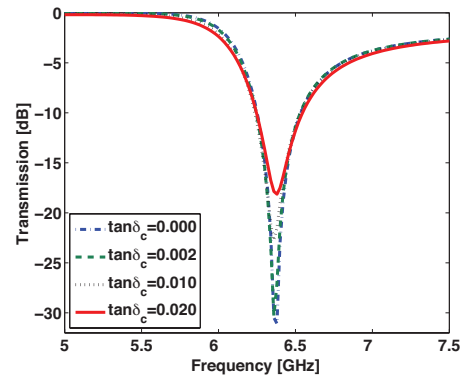
## 4. COMPARISON OF THE ELECTRICAL SIZES OF THE SRR, BC-SRR AND DSRR UNIT CELLS

Electrical size of a resonator cell is defined as

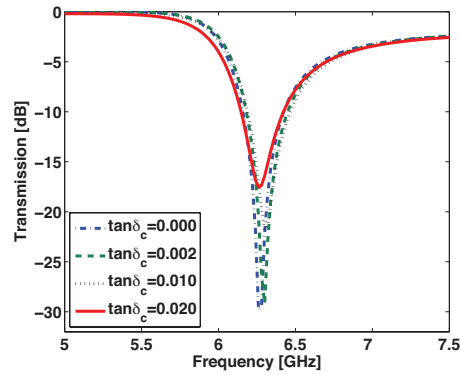
$$u = \frac{D}{\lambda_0} = \frac{D}{c/f_0} = f_0 \frac{D}{c} \quad (5)$$



(a) SRR case



(b) BC-SRR case



(c) DSRR case

**Figure 14.** Transmission spectra of the SRR, BC-SRR and DSRR unit cells for different loss tangent values of the substrate using  $L = 5$  mm,  $l = 4$  mm,  $h = 3$  mm,  $g = 0.5$  mm,  $w = 0.3$  mm,  $s = 0.5$  mm,  $d = 1.52$  mm and  $\epsilon_r = 4.4$ .

where  $D$  is the maximum linear dimension of the resonator, which is spatial diagonal  $\sqrt{h^2 + l^2} = \sqrt{3^2 + 4^2} = 5$  mm for all the rectangular unit cells simulated in this study;  $c$  is the velocity of light in vacuum and  $\lambda_0$  is the free space wavelength at the resonance frequency  $f_0$  [17]. Electrical size of a metamaterial unit cell is a very important property because of two reasons: First of all, smaller electrical size leads to more effective medium approximation and more accurate results from the quasi-static analysis [16]. Besides, electrically small materials are preferred in most of the microwave applications due to the miniaturization concern [17]. Using Equation (5) and the simulation results for  $f_0$  given in Figures 7 and 11, we can easily obtain  $u$  versus  $d$  and  $u$  versus  $\varepsilon_r$  curves for the SRR, BC-SRR and DSRR unit cells. As the electrical size  $u$  is proportional to the resonance frequency  $f_0$  as seen in Equation (5), the resulting electrical size curves are the same as the  $f_0$  versus  $d$  and  $f_0$  versus  $\varepsilon_r$  curves plotted in Figure 7 and Figure 11, apart from the proportionality constant ( $D/c$ ). The proper scale for the electrical size is indicated on the right border of those figures. It is obvious from these results that, the electrically smallest resonator structure for all  $d$  and  $\varepsilon_r$  values is DSRR unit cell with  $s = 0.2$  mm. It is also seen in Figure 7 that the DSRR topology with  $s = 0.5$  mm provides a reduction of 29 percent in the resonance frequency  $f_0$  as compared to the SRR topology with  $s = 0.5$  mm. In the case of  $s = 0.2$ , the reduction in  $f_0$  provided by the use of DSRR cell instead of SRR cell is 23 percent.

## 5. VERIFICATION OF THE EQUIVALENT CIRCUIT MODEL FOR DSRR

A simple equivalent circuit model is suggested for the DSRR unit cell in Section 2.2. In this section, we will verify that model as we have already completed the full wave electromagnetic simulations for the DSRR structure using the HFSS software. The equivalent circuits for the SRR structures used in our simulations have the inductance values of  $L = 14.4$  nH and  $L = 19$  nH for the cases of  $s = 0.5$  mm and  $s = 0.2$  mm, respectively, which are calculated using the inductance expression provided in [10] and they are expected to be independent of the substrate thickness and permittivity. The corresponding  $C$  values appearing in the SRR circuit blocks, on the other hand, are computed from the knowledge of  $L$  and  $f_0$  (of the SRR) for each set of substrate parameters. Finally, the parameters  $L_T, C_0, C_T$  and the resonance frequency  $f_0$  of the DSRR structure are computed using equations (1)–(4). The  $f_0$  values extracted for the DSRR unit cell for  $d = 0.51, 1.00, 1.52, 2.00$  mm with the parameter values of  $L = 5$  mm,

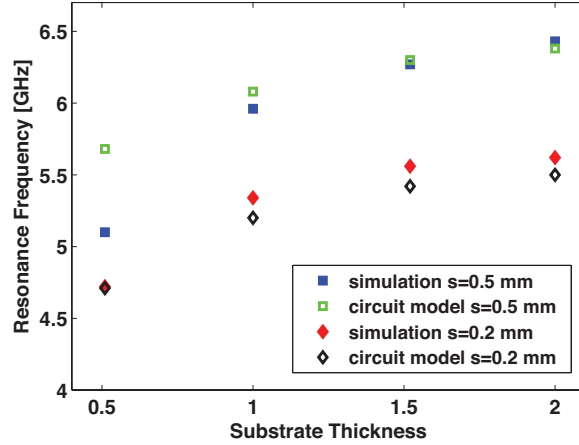


**Figure 15.** Resonance frequencies obtained from HFSS simulations and from the equivalent circuit model for different substrate thicknesses where  $\epsilon_r = 4.4$  and  $\tan \delta_c = 0.020$ .

$l = 4$  mm,  $h = 3$  mm,  $g = 0.5$  mm,  $w = 0.3$  mm,  $s = 0.5$  mm,  $\epsilon_r = 4.4$  and  $\tan c = 0.020$  are listed in Table 1 together with the corresponding  $f_0$  values. The HFSS-based and model-based  $f_0$  values of Table 1 are plotted in Figure 15. Similarly, Table 2 lists the  $f_0$  values of the DSRR cell obtained by using the HFSS software for  $\epsilon_r = 1, 2.5, 3.8, 4.1, 4.4, 4.7, 6.15$  and the parameter values  $L = 5$  mm,  $l = 4$  mm,  $h = 3$  mm,  $g = 0.5$  mm,  $w = 0.3$  mm,  $s = 0.5$  mm,  $d = 1.52$  mm and  $\tan c = 0.020$ . The corresponding model-based  $f_0$  values are also listed in Table 2. Again the HFSS-based and model-based  $f_0$  values of Table 2 are plotted in Figure 16. As it is seen in Table 1, Table 2 and Figures 15 and 16, the results of equivalent circuit model are found in very good agreement with the results of the HFSS simulations.

## 6. LEFT HANDED MEDIUM WITH DOUBLE SIDED SRR STRUCTURE

The DSRR unit cell can be combined with a conducting strip having the length of 5 mm, width of 0.5 mm, and thickness of 0.03 mm as shown in Figure 17 where the DSRR unit cell parameters are the same as those declared in section 2 with  $l = 4$  mm,  $h = 3$  mm,  $g = 0.5$  mm,  $w = 0.3$  mm,  $s = 0.5$  mm and the substrate parameters are taken as  $L = 5$  mm,  $d = 1.52$  mm,  $\epsilon_r = 4.4$  and  $\tan \delta_c = 0.020$ . For ordinary

**Table 1.** Resonance frequencies for the DSRR topology obtained from the HFSS simulations and from the equivalent circuit model for different substrate thicknesses ( $d$ ) where  $\varepsilon_r = 4.4$  and  $\tan \delta_c = 0.020$ .

$d$ [mm]	s=0.5 mm				s=0.2 mm			
	$f_0$ [GHz] HFSS	$f_0$ [GHz] Model	% error	C=C <sub>s</sub> /4 [pF]	$f_0$ [GHz] HFSS	$f_0$ [GHz] Model	% error	C=C <sub>s</sub> /4 [pF]
<b>0.51</b>	5.10	5.68	11.4	0.030	4.72	4.71	0.2	0.032
<b>1.00</b>	5.96	6.08	2.0	0.035	5.34	5.20	2.6	0.035
<b>1.52</b>	6.27	6.30	0.5	0.036	5.56	5.42	2.5	0.036
<b>2.00</b>	6.43	6.38	0.8	0.037	5.62	5.50	2.1	0.037

**Table 2.** Resonance frequencies for the DSRR topology obtained from the HFSS simulations and from the equivalent circuit model for different values of the relative substrate permittivity ( $\varepsilon_r$ ) where  $d = 1.52$  mm and  $\tan \delta_c = 0.020$ .

$\varepsilon_r$	s=0.5 mm				s=0.2 mm			
	$f_0$ [GHz] HFSS	$f_0$ [GHz] Model	% error	C=C <sub>s</sub> /4 [pF]	$f_0$ [GHz] HFSS	$f_0$ [GHz] Model	% error	C=C <sub>s</sub> /4 [pF]
<b>1</b>	10.34	10.49	1.5	0.014	9.04	9.05	0.1	0.014
<b>2.5</b>	7.84	7.82	0.3	0.024	6.92	6.75	2.5	0.024
<b>3.8</b>	6.68	6.62	0.9	0.033	5.86	5.76	1.7	0.032
<b>4.1</b>	6.48	6.42	0.9	0.035	5.74	5.58	2.8	0.034
<b>4.4</b>	6.27	6.30	0.5	0.036	5.56	5.42	2.5	0.036
<b>4.7</b>	6.10	6.07	0.5	0.039	5.38	5.27	2.0	0.038
<b>6.15</b>	5.46	5.39	1.3	0.049	4.86	4.7	3.2	0.047

SRR structures the conducting strip is printed over the back side of the substrate, which is not suitable for BC-SRR or DSRR structures. For these double sided structures, embedding the conducting strip inside the substrate is feasible using a high resolution LPKF milling machine. With this convenient and inexpensive manufacturing approach, it is possible to combine two substrates with SRR patterns printed on their outer faces and anti-symmetrically aligned with respect to each other while only one of the substrates has the conducting strip printed on its inner side facing the second substrate. In other words, manufacturing the metamaterial structure seen in Figure 17 is not too complicated

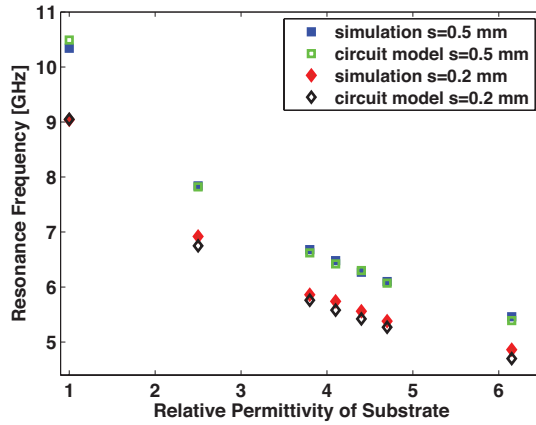


**Figure 16.** Resonance frequencies obtained from HFSS simulations and from the equivalent circuit model for different relative substrate permittivities where  $d = 1.52$  mm and  $\tan \delta_c = 0.020$ .

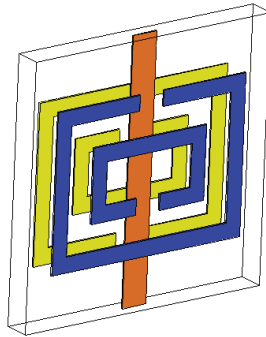


**Figure 17.** Left-handed unit-cell composed of a DSRR and a conducting strip.

but quite feasible.

The  $S_{11}$  and  $S_{21}$  spectra of the periodic structure associated with the metamaterial unit cell given in Figure 17 are simulated by HFSS using the specific boundary conditions explained in detail in Section 2.1, to extract the complex effective medium parameters  $\epsilon_{eff}$  and  $\mu_{eff}$  over the frequency band of simulation [24]. The method given in [13] is used for effective parameter retrieval. Real and imaginary parts of the effective permittivity and effective permeability parameters are plotted in Figure 18 to demonstrate that the suggested DSRR with

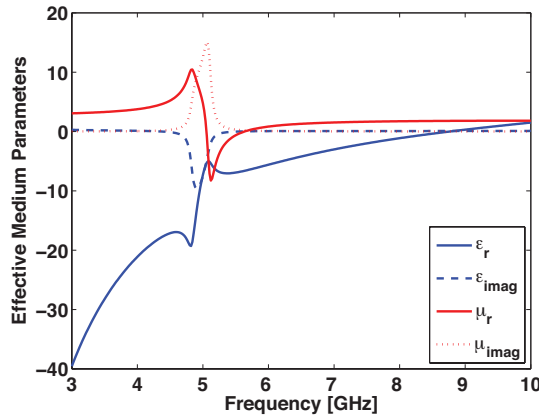


**Figure 18.** Real and imaginary parts of effective medium parameters for the structure given in Figure 17.

conducting strip structure has negative permittivity and permeability over the frequency band from 5.05 GHz to 5.64 GHz. In other words, the suggested DSRR resonator topology is also useful to design a left handed metamaterial, if needed.

## 7. CONCLUSION

In this paper, we have suggested a new  $\mu$ -negative (MNG) metamaterial structure, the double-sided SRR (DSRR), which combines the topological properties of the previously suggested BC-SRR and the conventional SRR to achieve much a smaller resonance frequency (i.e., a much smaller electrical size) for a fixed set of cell dimensions. In other words, the DSRR structure can provide much better miniaturization in RF design applications while satisfying the condition for effective medium approach. The suggested DSRR cell has also been demonstrated as having a much wider half power resonance bandwidth as compared to the conventional SRR cell. The bandwidth performance of the DSRR cell approaches to that of the BC-SRR cell as the separation between the inner and outer rings increases. Our full-wave electromagnetic simulations by HFSS have also demonstrated that the depth of the resonance curve increases as the substrate gets thicker. Finally, the combination of the DSRR cell and a conducting strip has shown to provide a left-handed metamaterial behavior, as expected.

A simple electrical circuit model is also proposed and verified to approximately describe the relation between substrate parameters

(substrate thickness and substrate relative permittivity) and the resonance frequency. As a future work, we will improve the circuit model for the DSR structure to account for the conductor and dielectric losses. Also, it has been shown in literature that multiple SRR (MSRR) structures and spiral resonators (SR) with larger number of turns provide better miniaturization [10, 17, 21, 22] as compared to conventional SRRs with just two rings. As a future work, we will investigate the double-sided multiple SRR, double sided spiral resonator and double sided U-spiral structures with large number of rings to see if further miniaturization is possible due to double-sided topologies with strong broadside coupling effects.

## REFERENCES

1. Veselago, V. G., "The electrodynamics of substances with simultaneously negative values of  $\epsilon$  and  $\mu$ ," *Sov. Phys. Usp.*, Vol. 10, 509–514, 1968.
2. Pendry, J. B., A. J. Holden, D. J. Robbins, and W. J. Stewart, "Low frequency plasmons in thin-wire structures," *J. Phys.: Condens. Matter*, Vol. 10, 4785–4809, 1998.
3. Pendry, J. B., A. J. Holden, D. J. Robbins, and W. J. Stewart, "Magnetism from conductors and enhanced nonlinear phenomena," *IEEE Trans. Microwave Theory Tech.*, Vol. 47, No. 11, 2075–2084, 1999.
4. Smith, D. R., W. J. Padilla, D. C. Vier, S. C. Nemat-Nasser, and S. Schultz, "Composite medium with simultaneously negative permeability and permittivity," *Phys. Rev. Lett.*, Vol. 84, No. 18, 4184–4187, 2000.
5. Weiland, T., R. Schuhmann, R. B. Greegor, C. G. Parazzoli, A. M. Vetter, D. R. Smith, D. C. Vier, and S. Schultz, "Ab initio numerical simulation of left-handed metamaterials: Comparison of calculation and experiments," *J. Appl. Phys.*, Vol. 90, No. 10, 5419–5424, 2001.
6. Aydin, K., I. Bulu, K. Guven, M. Kafesaki, C. M. Soukoulis, and E. Ozbay, "Investigation of magnetic resonances for different split-ring resonator parameters," *New Journal of Physics*, Vol. 7, No. 168, 1–15, 2005.
7. Sheng, Z. and V. V. Varadan, "Tuning the effective properties of metamaterials by changing the substrate properties," *J. Appl. Phys.*, Vol. 101, 014909 (1)–(7), 2007.
8. Baena, J. D., R. Marqués, F. Medina, and J. Martel, "Artificial

- magnetic metamaterial design by using spiral resonators,” *Phys. Rev. B*, Vol. 69, 014402(1)–(5), 2004.
9. Chen, H., L. Ran, J. Huangfu, T. M. Grzegorzczuk, and J. A. Kong, “Equivalent circuit model for left-handed metamaterials,” *J. Appl. Phys.*, Vol. 100, 024915(1)–024915(6), 2006.
  10. Bilotti, F., A. Toscano, L. Vegni, K. Aydin, K. B. Alici, and E. Ozbay, “Equivalent-circuit models for the design of metamaterials based on artificial magnetic inclusions,” *IEEE Trans. Microwave Theory Tech.*, Vol. 55, No. 12, 2865–2873, 2007.
  11. Marqués, R., F. Medina, and R. Rafii-El-Idrissi, “Role of bianisotropy in negative permeability and left-handed metamaterials,” *Phys. Rev. B*, Vol. 65, 14440(1)–14440(6), 2002.
  12. Marqués, R., F. Mesa, J. Martel, and F. Medina, “Comparative analysis of edge- and broadside-coupled split ring resonators for metamaterial design-theory and experiments,” *IEEE Trans. Antennas Propag.*, Vol. 51, No. 10, 2572–2581, 2003.
  13. Ghodgaonkar, D. K., V. V. Varadan, and V. K. Varadan, “Free-space measurement of complex permittivity and complex permeability of magnetic materials at microwave frequencies,” *IEEE Trans. Instrum. Meas.*, Vol. 39, No. 2, 387–394, 1990.
  14. Baena, J. D., J. Bonache, F. Martín, R. M. Sillero, F. Falcone, T. Lopetgi, M. A. G. Laso, J. García-García, I. Gil, M. F. Portillo, and M. Sorolla, “Equivalent-circuit models for split-ring resonators and complementary split-ring resonators coupled to planar transmission lines,” *IEEE Trans. Microwave Theory Tech.*, Vol. 53, No. 4, 1451–1461, 2005.
  15. Ekmekci, E. and G. Turhan-Sayan, “Sensitivity of the resonance characteristics of SRR and DSRR (double-sided SRR) type metamaterials to the changes in substrate parameters and the usefulness of DSRR structure for reduced electrical size,” *PIERS Proceedings*, 598–602, Cambridge, USA, July 2008.
  16. Zhao, H. and T. J. Cui, “A double-spiral resonator structure to realize left-handed material with lower resonant frequency,” *Microw. Opt. Technol. Lett.*, Vol. 48, No. 5, 923–926, 2006.
  17. Alici, K. B., F. Bilotti, L. Vegni, and E. Ozbay, “Miniaturized negative permeability materials,” *Appl. Phys. Lett.*, Vol. 91, 071121(1)–(3), 2007.
  18. Wu, B., B. Li, T. Su, and C.-H. Liang, “Equivalent-circuit analysis and lowpass filter design of split-ring resonator DGS,” *J. of Electromagn. Waves and Appl.*, Vol. 20, No. 14, 1943–1953, 2006.
  19. Yao, H.-Y., L.-W. Li, Q. Wu, and J. A. Kong, “Macroscopic per-

- formance analysis of metamaterials synthesized from microscopic 2-D isotropic cross split-ring resonator array,” *Progress In Electromagnetics Research*, PIER 51, 197–217, 2005.
20. Cui, T. J., H. F. Ma, R. Liu, B. Zhao, Q. Cheng, and J. Y. Chin, “A symmetrical circuit model describing all kinds of circuit metamaterials,” *Progress In Electromagnetics Research B*, Vol. 5, 63–76, 2008.
  21. Aznar, F., M. Gil, J. Bonache, J. García-Garca, and F. Martin, “Metamaterial transmission lines based on broad-side coupled spiral resonators,” *Electron. Lett.*, Vol. 43, No. 9, 2007.
  22. Aznar, F., J. García-Garca, M. Gil, J. Bonache, and F. Martin, “Strategies for the miniaturization of metamaterial resonators,” *Microw. Opt. Technol. Lett.*, Vol. 50, No. 5, 1263–1270, 2008.
  23. Ziolkowski, R. W., “Design, fabrication, and testing of double negative metamaterials,” *IEEE Trans. Antennas Propag.*, Vol. 51, No. 7, 2003.
  24. Wu, B.-I., W. Wang, J. Pacheco, X. Chen, T. Grzegorzcyk, and J. A. Kong, “A study of using metamaterials as antenna substrate to enhance gain,” *Progress In Electromagnetics Research*, PIER 51, 295–328, 2005.
  25. Ekmekci, E. and G. Turhan-Sayan, “Reducing the electrical size of magnetic metamaterial resonators by geometrical modifications: A comparative study for single-sided and double-sided multiple SRR, spiral and U-spiral resonators,” *IEEE AP-S International Symposium on Antennas and Propagation*, July 2008, San Diego, USA.